

Dynamic Instability in a DNA-Segregating Prokaryotic Actin Homolog

Ethan C. Garner,* Christopher S. Campbell,* R. Dyche Mullins†

Dynamic instability—the switching of a two-state polymer between phases of steady elongation and rapid shortening—is essential to the cellular function of eukaryotic microtubules, especially during chromosome segregation. Since the discovery of dynamic instability 20 years ago, no other biological polymer has been found to exhibit this behavior. Using total internal reflection fluorescence microscopy and fluorescence resonance energy transfer, we observe that the prokaryotic actin homolog ParM, whose assembly is required for the segregation of large, low-copy number plasmids, displays both dynamic instability and symmetrical, bidirectional polymerization. The dynamic instability of ParM is regulated by adenosine triphosphate (ATP) hydrolysis, and filaments are stabilized by a cap of ATP-bound monomers. ParM is not related to tubulin, so its dynamic instability must have arisen by convergent evolution driven by a set of common constraints on polymer-based segregation of DNA.

Recent work suggests that proteins related to eukaryotic actins (*I–3*) may be involved in prokaryotic chromosome segregation. Another example of prokaryotic DNA segregation, one that has been characterized in molecular detail, is the partitioning of R1 and R100 drug-resistance plasmids. These 100-kb plasmids are found in many enteric pathogens and encode genes that confer antibiotic and heavy-metal resistance as well as genes required for plasmid retention and conjugative transfer. They are stably maintained at two to four copies per cell (*4*) and have evolved an efficient mechanism to ensure inheritance by both daughters during cell division. The R1 *par* operon appears to construct a minimalist mitotic spindle from three components—*parC*, ParR, and ParM (*5–7*)—that positions pairs of plasmids at opposite ends of a rod-shaped bacterium (*8*). *parC* is a stretch of centromeric DNA that includes the R1 *par* promoter sequence (*9*); ParR is a repressor protein that binds to the *parC* locus (*9*); and ParM is an actin homolog. Purified ParM polymerizes in an ATP-dependent manner (*7*) into two-stranded helical filaments similar to conventional actin filaments (*10*) and binds specifically to the ParR-*parC* complex (*8*). In vivo, ParM filaments form a bundle that extends the length of the bacterium with plasmid DNA localized at each end, and polymerization of ParM has been postulated to provide force to push plasmids to opposite poles of the cell

(*7, 8*). Because the system contains only three components, we hypothesized that the intrinsic assembly dynamics of ParM are critical to its role in segregating DNA.

We first investigated the kinetic polarity of ParM filament assembly by performing dual-color fluorescence microscopy on ParM filaments assembled in vitro. Both actin filaments and microtubules are structurally and kinetically polarized so that one end of the polymer elongates faster than the other, and ultrastructural studies indicate that ParM filaments have a structural polarity similar to that of actin filaments (*10*). We polymerized filaments labeled with Alexa 488 (green) by adding the nonhydrolyzable ATP analog adenylylimidodiphosphate (AMP-PNP), and then added Cy3-labeled (red) ParM. Most filaments observed (91%) had green centers with equal amounts of red fluorescence on each end (Fig. 1A); this result suggested that, unlike previously characterized nucleotide-dependent polymers, ParM filament polymerization is kinetically symmetrical.

We next examined the polymerization dynamics of individual ParM filaments by total internal reflection fluorescence (TIRF) microscopy of Alexa 488-labeled ParM. In the presence of AMP-PNP, ParM filaments were very long (Fig. 1B, left) and grew symmetrically with equal rates of assembly at each end (Fig. 1C) (movies S1 and S2). Electron microscopy of polymeric ParM revealed well-separated, individual filaments with no obvious bundles (*7, 10*). This observation, together with the approximately uniform fluorescence along the length of labeled ParM filaments, implies that we are observing individual filaments and not antiparallel bundles of asymmetrically elongating filaments. In

the presence of hydrolyzable ATP, ParM filaments also elongated symmetrically but were much shorter (Fig. 1B, right) and more dynamic (movies S3 to S5). After growing for a variable length of time, ATP-ParM filaments abruptly switched from bidirectional elongation to rapid, endwise disassembly (Fig. 1D). In most cases disassembly was unidirectional, and in all cases observed ($n > 530$), the switch from elongation to shortening resulted in complete disassembly of the filament. Shortening did not reflect detachment of the filament from the coverslip, as detachment resulted in disappearance of the filament in a single step (*11*). At all ParM concentrations above 2 μM the average filament length was 1.5 μm , which suggests that length is determined primarily by an intrinsic property of the filaments (Fig. 1F). ATP-ParM filaments elongated with a rate constant of $5.3 \pm 1.3 \mu\text{M}^{-1} \text{s}^{-1}$ ($n = 50$) at each end, similar to that of the fast-growing barbed end of actin filaments. After switching from growth to shortening, filaments disassembled at a rate of $64 \pm 20 \text{s}^{-1}$ ($n = 16$) (Fig. 1E). The time spent growing and the maximum length achieved before catastrophic disassembly were variable, which suggests that the switch from elongation to shortening is stochastic. This property of switching between phases of elongation and rapid shortening, known as dynamic instability (*12*), has until now been observed only in eukaryotic microtubules.

ParM filaments, like microtubules and conventional actin filaments, assemble via a nucleation-condensation mechanism characterized by (i) the existence of a critical concentration, above which polymer forms and below which it does not, and (ii) a concentration-dependent time lag in spontaneous polymerization, during which stable nuclei assemble. We used fluorescence resonance energy transfer (FRET) to monitor ParM polymerization kinetics at varying concentrations of protein and ATP [see (*11*) for assay conditions and control experiments]. Using both FRET and high-speed pelleting assays, we determined an apparent steady-state critical concentration of 2.3 μM for Mg^{2+} -ATP ParM (see below) (fig. S3A). This value is consistent with estimates based on fluorescence microscopy (Fig. 1F). In addition, ATP-induced polymerization of ParM filaments proceeded after a time lag that decreased with increasing protein concentration (Fig. 2A, inset) (fig. S3B).

We define the filament nucleus as the smallest oligomer more likely to elongate than to fall apart. By this definition, the maximum rate of polymer assembly is approximately $k_{e+}k_{n+}[m^*]^n$, where $[m^*]$ is the initial monomer concentration minus the critical concentration, k_{e+} is the rate constant for polymer elongation, k_{n+} is the rate constant for the nucleation reaction, and n

University of California, 600 16th Street, San Francisco, CA 94107, USA.

*These authors contributed equally to this work.

†To whom correspondence should be addressed.
E-mail: dyche@mullinslab.ucsf.edu

is the number of monomers required to form a nucleus (13). By plotting the logarithm of the maximum rate of polymerization versus the logarithm of the protein concentration (13, 14), we determined that conventional actin and ParM both elongate from a nucleus composed of three monomers (Fig. 2A), as

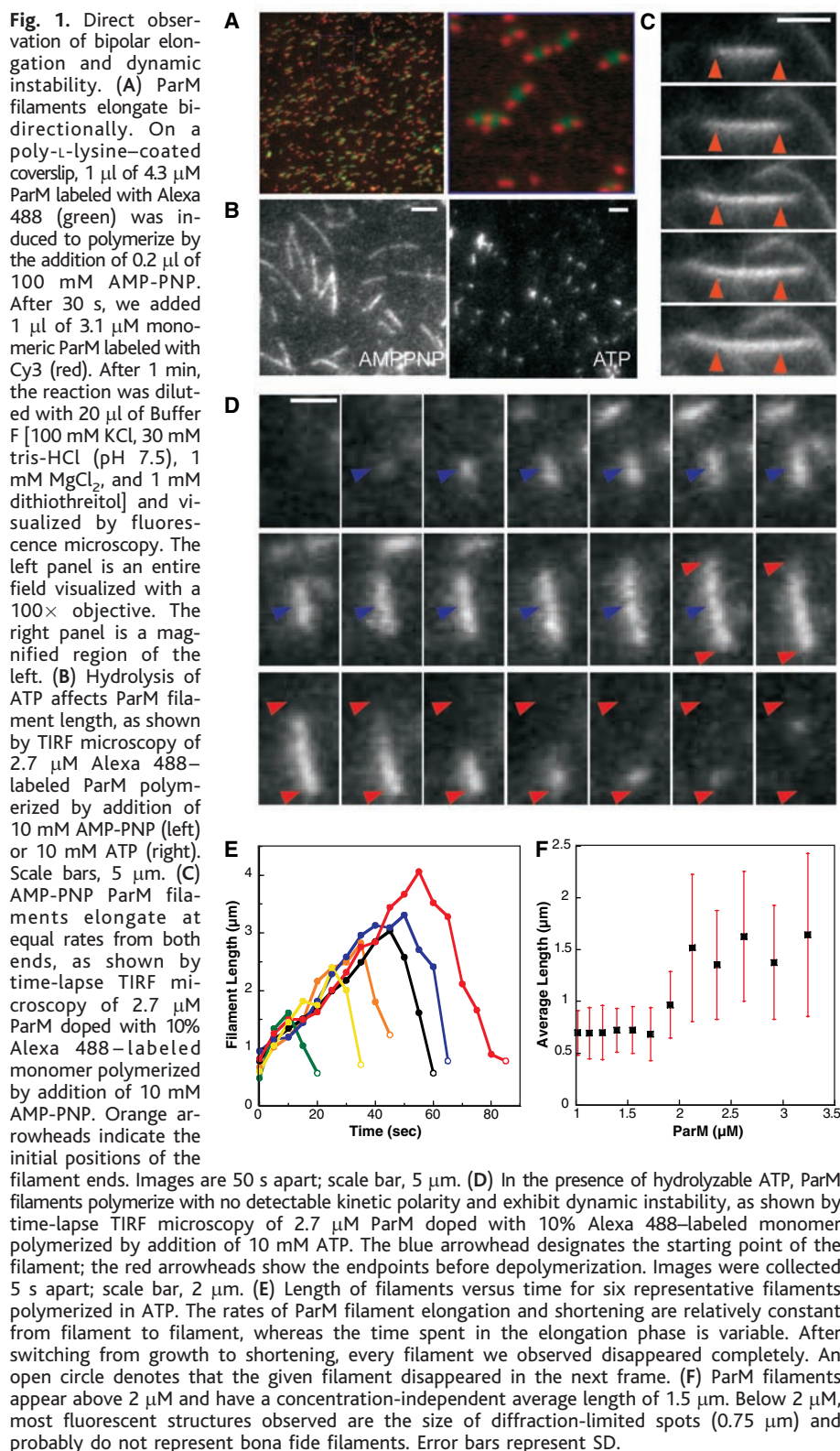
expected for a two-stranded, helical polymer (15). Although the slopes are identical, the ParM polymerization data are shifted upward by about 2.5 log units relative to the data for conventional actin. This indicates that the product of the nucleation and elongation rates is higher for ParM than for actin by a factor

of 300. Because the elongation rates are approximately equal, the shift in the ParM data must reflect a spontaneous nucleation rate 300 times the rate for conventional actin.

Consistent with previous studies (7), we found that the half-life of ParM filaments in solution increased linearly with increasing concentration of ATP, which suggests that polymer stability is regulated by ATP hydrolysis (Fig. 2B). The bulk assembly kinetics of ParM were triphasic, with an initial peak in polymer concentration followed by a dip and then a slow approach to equilibrium [see (11) for further discussion of polymerization kinetics]. The initial rise and fall in ParM polymer appears to represent a population of rapidly nucleated filaments that elongate in synchrony and undergo somewhat synchronous catastrophe. Microtubules exhibit similar synchronous behavior under conditions where nucleation is fast and/or nucleotide dissociation is slow (16, 17).

Consistent with the notion that ATP hydrolysis regulates ParM filament stability, we found that ADP-ParM filaments are extremely unstable, with a critical concentration of $\sim 100 \mu\text{M}$ (18). To determine whether hydrolysis of ATP itself or dissociation of cleaved phosphate destabilizes the filament, we tested the effect of beryllium fluoride (BeF_3), a phosphate analog, on ParM filament stability. BeF_3 has been used to stabilize ADP actin filaments (19), and it appears to induce a conformation similar to that of filaments after cleavage of the γ -phosphate of the bound ATP but before phosphate dissociation ($\text{ADP}\cdot\text{P}_i$). Addition of BeF_3 and ADP did not induce assembly of ParM filaments, but BeF_3 did stabilize filaments formed in low concentrations of ATP (Fig. 2C). TIRF microscopy revealed that the length distribution of BeF_3 -ParM filaments was identical to that of ATP-ParM filaments (fig. S1A), but BeF_3 -ParM filaments did not exhibit dynamic instability (movie S6). By FRET assays, the critical concentration of BeF_3 -ParM is $0.6 \mu\text{M}$ (Fig. 3B). It appears that the steady-state monomer concentration that we measure for ATP ParM ($2.3 \mu\text{M}$) is the sum of the critical concentrations of the ATP- and ADP-filament ends weighted by their relative abundance.

Polymerization of ParM stimulates hydrolysis of bound ATP (7), so we directly compared the kinetics of ParM polymerization and ATP hydrolysis in side-by-side assays. To measure polymerization, we mixed labeled ParM ($15 \mu\text{M}$) with $200 \mu\text{M}$ ATP in a rapid mixer and recorded the FRET signal (Fig. 2D). To measure hydrolysis, we mixed material from the same sample with $200 \mu\text{M}$ ATP doped with γ - ^{32}P ATP in a quenched-flow rapid mixing device. Hydrolysis followed filament assembly, and the instantaneous rate of hydrolysis was proportional to the measured polymer concentration (Fig. 2D, inset).



The hydrolysis stimulated by polymerization was rapid, with a rate constant of 0.2 s^{-1} . This is similar to the rates of hydrolysis in actin filaments (0.3 s^{-1}) (20) and in polymers of the bacterial tubulin homolog ftsZ (0.13 s^{-1}) (21) and is fast enough to account for the observed rapid dynamics of ParM filaments. Complete loss of ParM polymer did not correlate with complete exhaustion of ATP in the reaction, which suggests that low concentrations of ADP generated in the reaction inhibit polymerization of ParM. Further work revealed that free ADP affects ParM filament stability (11). All of our observations of intrinsic dynamic instability were made under conditions where this additional ADP-dependent destabilizing effect was not observed.

To determine conclusively whether nucleotide hydrolysis drives dynamic instability of ParM filaments, we mutated residues required for ATP hydrolysis by ParM and tested the effect on filament stability. On the basis of the model of Vorobiev *et al.* for ATP hydrolysis by actin (22), we mutated Glu¹⁴⁸ of ParM to Ala (fig. S4A) and tested the effect on polymerization and ATP hydrolysis (11). This mutation (E148A) abolished all detectable ATPase activity, even at high protein concentrations (Fig. 3A, inset). Like wild-type ParM, the E148A mutant assembled into filaments in a symmetrical bidirectional manner (movie S7); however, unlike wild-type ParM, E148A filaments were stable in low ATP concentrations (Fig. 3A). TIRF microscopy revealed that E148A-ParM filaments are long and stable in the presence of ATP, similar to wild-type ParM filaments formed in the presence of AMP-PNP (fig. S4B). Nucleation of E148A-ParM filaments was slower than that of wild-type filaments, but once formed, mutant filaments elongated at the same rate as wild-type filaments (fig. S4D). Finally, the critical concentration of the E148A mutant ($0.68 \mu\text{M}$) was close to that of BeF₃-bound wild-type ParM ($0.6 \mu\text{M}$) (Fig. 3B).

A basic assumption of nucleotide-dependent dynamic instability is that the polymer is stable as long as the ends retain a cap of nucleotide triphosphate-bound monomers (23, 24). Once this cap is lost, the polymer rapidly depolymerizes. To determine whether ParM filaments are stabilized by an ATP cap, we mixed wild-type and E148A ParM in different ratios to determine whether substoichiometric amounts of E148A can stabilize wild-type ParM filaments. In pelleting experiments, small amounts of E148A decreased the critical concentration of wild-type ParM (Fig. 3C). Above 20% E148A, the total amount of ParM in the supernatant fraction remained constant and was close to the measured critical concentration of the E148A mutant. This result suggests that subsaturating amounts of ATP-bound ParM can stabilize wild-type

polymer, consistent with the ability of an ATP cap to stabilize ADP-bound filaments.

TIRF microscopy assays also revealed that small amounts of E148A ParM affects filament stability. Filaments doped with 20% E148A were very stable (fig. S4C) and elongated in a bipolar fashion, similar to filaments composed entirely of E148A (movie S8). Samples with 10% E148A contained a subset of filaments that remained stable for long periods of time. At 3% and 5% E148A, fewer filaments were stable, and samples doped with 1% E148A were identical to wild-type ParM. At dopings of 3% and 5%, we observed filaments that experienced periods of elongation and rapid shortening but did not undergo complete disassembly (Fig. 3D). This behavior is similar to the

phenomenon of “rescue” observed in dynamic instability of microtubules.

We note three important differences between the kinetics of ParM filament assembly and those of conventional actin. First, the rate of dissociation of ADP-ParM monomers from filament ends is about 100 times the rate for ADP-actin monomers from the pointed end (Table 1). ADP-actin filaments require severing factors such as cofilin to promote complete disassembly (25), whereas the fast off-rate of ADP-ParM monomers from the end of the filament produced a microtubule-like dynamic instability (Fig. 4A). Second, the nucleation rate of ParM filaments is 300 times the rate for actin filaments. Evolution has erected a large kinetic barrier to spontaneous nucleation of

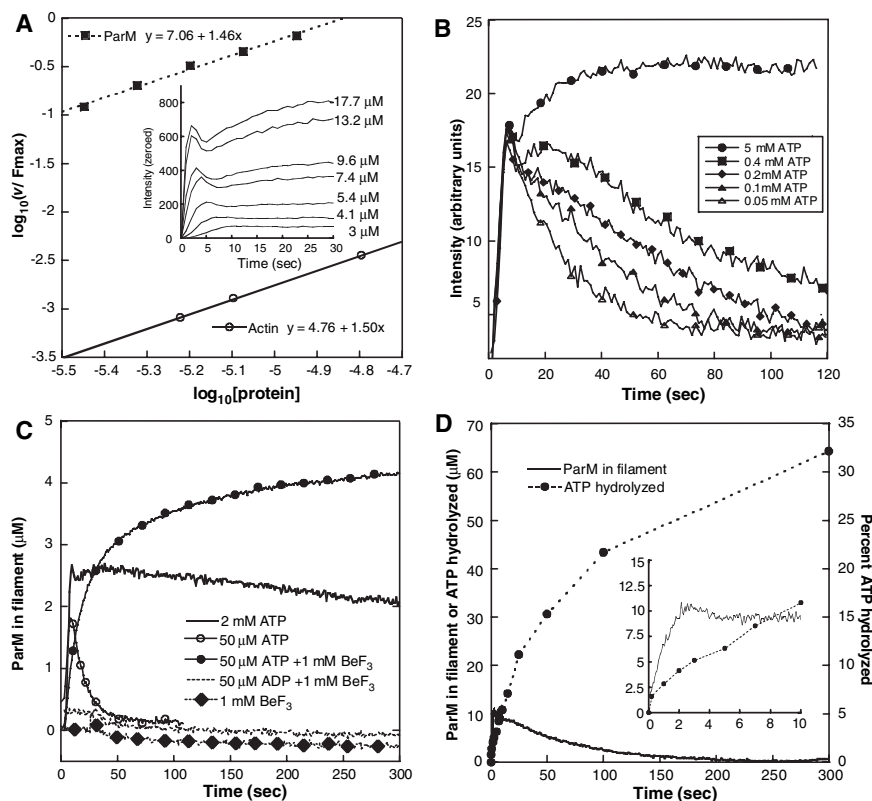


Fig. 2. Kinetics of ParM polymerization measured by FRET. (A) Determination of the nucleus size and relative nucleation rates of ParM and conventional actin filaments. FRET-labeled ParM (unlabeled ParM doped with 15% Cy3- and 15% Cy5-labeled monomer) was polymerized at varying concentrations by the addition of 5 mM ATP (inset). The maximal velocity of the polymerization signal was divided by the maximal fluorescence, and the log of this value was plotted against the log of the concentration of protein. The lines in the graph have a slope proportional to $(n - 1)$, where n is the nucleus size, and the x intercept is the relative nucleation rate (k_{n+}). This analysis shows that ParM and actin both elongate from nuclei composed of three monomers and that the spontaneous nucleation rate of ParM filaments is 300 times that of actin. (B) The lifetime of ParM filaments depends on ATP concentration. We used a rapid mixer to combine 5 μM FRET-labeled ParM with the indicated amount of ATP and monitored polymer content by FRET. (C) The phosphate analog BeF₃ stabilizes ParM filaments. We used a rapid mixer to combine 5 μM FRET-labeled ParM with ADP or ATP in the presence or absence of 1 mM BeF₃ and monitored polymer content by FRET. (D) ATP hydrolysis lags behind ParM polymerization. To monitor polymerization and ATP hydrolysis, we mixed 15 μM FRET-labeled ParM with 200 μM ATP doped with [γ -³²P]ATP. We monitored polymerization by mixing in a stopped-flow rapid mixer and monitoring FRET. We monitored ATP hydrolysis by mixing the samples in a quenched-flow rapid mixer and measuring the amount of radioactive phosphate released at various time points. Total polymer and cleaved phosphate are plotted on the same scale. (Inset) Expansion of the first 10 s of the plot.

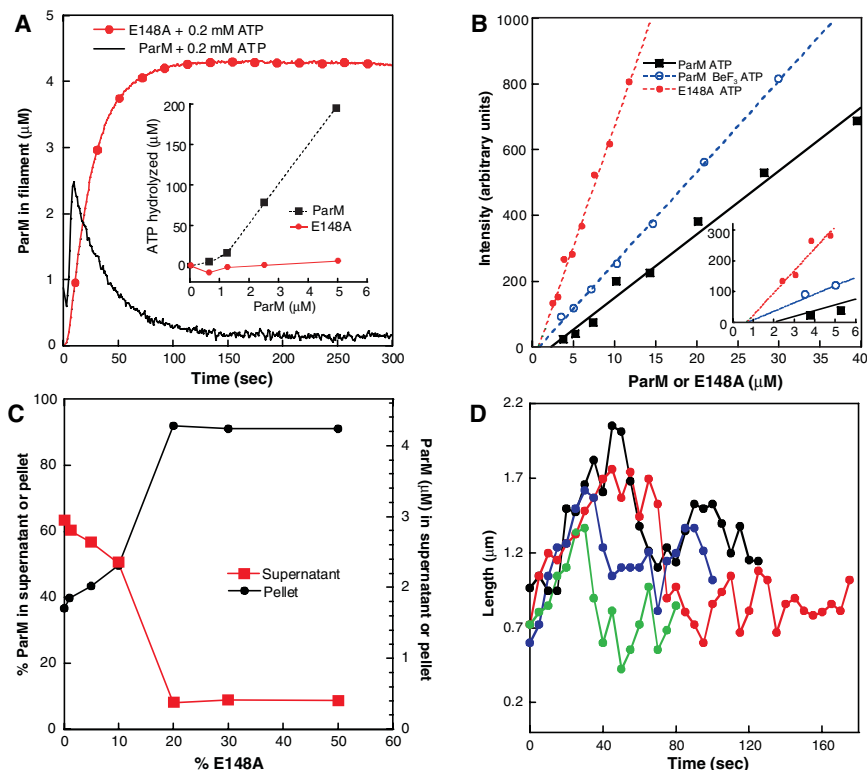


Fig. 3. Small amounts of nonhydrolyzing mutant ParM stabilize wild-type ParM filaments. (A) Mutating Glu¹⁴⁸ of ParM to alanine (E148A) abolishes hydrolysis of ATP and stabilizes ParM filaments. We measured polymerization kinetics by FRET using 5 μM FRET-labeled E148A or wild-type ParM. We used a stopped-flow rapid mixer to induce polymerization with 200 μM ATP. Inset: Bulk measurements of ATP hydrolysis by wild-type and E148A ParM. The indicated concentrations of wild-type or E148A ParM were combined with 1 mM ATP doped with [γ -³²P]ATP. The amount of cleaved radioactive phosphate was determined after 15 min. (B) The critical concentrations of the ATP (ATP + E148A) and ADP-Pi (ATP + BeF₃ + ParM) states are one-fourth the apparent ATP-ParM critical concentration. Serially diluted FRET-labeled wild-type ParM or E148A (95 μl in each case) was combined with 5 mM ATP or 5 mM ATP plus 1 mM BeF₃ within a cuvette. The unpolymerized signal was subtracted from the polymerized signal and plotted against the concentration of protein. The x-intercept values are taken as the critical concentrations. (C) Substoichiometric amounts of the hydrolysis-deficient ParM mutant stabilize ParM filaments. Cy3-labeled ParM (5.1 μM) was combined with Cy5-labeled E148A (5.1 μM) in the indicated ratios, polymerized with 10 mM ATP, and spun in an ultracentrifuge. Samples of supernatant and pellet were analyzed by SDS-polyacrylamide gel electrophoresis and quantitated with a fluorescent imager. Graph indicates the amounts of Cy3-ParM fluorescence. In the absence of E148A mutant ParM, the critical concentration of ParM is 2.7 μM . Addition of low concentrations of E148A ParM decreases the critical concentration. At 20% doping of the mutant, the critical concentration falls to \sim 0.5 μM —the critical concentration of E148A ParM alone. (D) Substoichiometric concentrations of E148A ParM promote rescue of depolymerizing ParM filaments. We plotted filament length versus time for four individual filaments (indicated by four colors) composed of 5% E148A and 95% wild-type ParM. Time zero corresponds to the initiation of a period of elongation. Unlike filaments composed entirely of wild-type ParM, the composite filaments oscillate in length and the switch from elongation to shortening does not always result in complete filament disassembly.

eukaryotic actins, so that actin requires nucleation factors such as the Arp2/3 complex (26) and formins (27) to form filaments *in vivo*. The rate of the spontaneous ParM filament formation is similar to that of conventional actin in the presence of formins (28). Third, the rate of ADP dissociation from ParM monomers is 100 times as fast as from actin, which requires profilin to achieve the same rate of nucleotide dissociation and exchange (25). Thus, ParM appears to be kinetically tuned to operate independently of exogenous nucleation, depolymerization, and nucleotide exchange factors.

Both ParM filaments and microtubules segregate DNA, and both exhibit dynamic instability. Dynamic instability of tubulin is driven by guanosine triphosphate hydrolysis; during mitosis, dynamic instability enables the ends of microtubules to search intracellular space efficiently and to locate kinetochores of unattached chromosomes [for a review, see (29)]. Dynamic instability of ParM filaments is driven by ATP hydrolysis, and mutations in ParM that perturb nucleotide hydrolysis abolish plasmid partitioning (30, 31), which suggests that ParM dynamic instability is required for plasmid segrega-

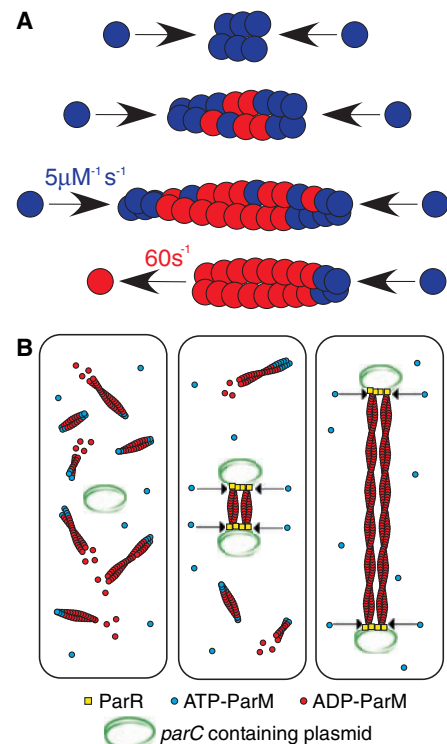


Fig. 4. Model for dynamic instability and *in vivo* function of ParM filaments. (A) Kinetic model for the dynamic instability of ParM. Once a nucleus is formed, the polymer elongates in a kinetically symmetrical manner. Polymerization induces ATP hydrolysis and ADP-bound monomers accumulate in the center of the filament. The filament remains stable as long as it maintains an ATP cap at both ends. When the cap at one end is lost, the polymer rapidly disassembles from that end. (B) Model for ParM-mediated plasmid segregation. ParM filaments spontaneously nucleate and elongate throughout the cell. Because of hydrolysis-induced dynamic instability, these polymers are unstable and they rapidly disassemble. Upon plasmid replication, two ParR-*parC* complexes form and are competent to capture and stabilize both ends of a set of ParM filaments. Through a mechanism of insertional polymerization at the ParM-ParR interface (arrows), the spindle elongates bidirectionally and pushes plasmids to the opposing ends of the cell.

tion. We hypothesize that ParM dynamic instability enables filament ends to efficiently locate and capture plasmid DNA targets. The average length of ATP-ParM filaments (1.5 μm) is comparable to the length of many rod-shaped bacteria, so ParM filaments may be kinetically tuned to search the volume of a bacterial cell and capture ParR-*parC* complexes. In addition, bidirectional assembly would promote segregation without requiring antiparallel filaments to slide past each other.

Møller-Jensen *et al.* (7) reported that the ParR-*parC* complex nucleates ParM polymerization. Their data, however, show only that ParR-*parC* can stabilize ParM filaments below the steady-state ATP critical concentration. Given the low nucleation barrier and

Table 1. Kinetic parameters of ParM and actin. All values are for the Mg²⁺-bound form unless otherwise indicated. *K_d*, dissociation constant.

Parameter	Actin	ParM	Method
Steady-state ATP critical concentration (Mg ²⁺)	100 nM	2.3 μM	Pelleting, FRET assay, microscopy
Steady-state ATP critical concentration (Ca ²⁺)	440 nM (in 100 mM KCl)	6.8 μM	Pelleting
ATP critical concentration	Barbed end: 100 nM Pointed end: 600 nM	550 to 680 nM	FRET assay (BeF-ATP-ParM and ATP-E148A)
ADP critical concentration	1 μM	~100 μM	Pelleting
ATP-monomer on-rate	Barbed end: 10 μM ⁻¹ s ⁻¹ Pointed end: 1 μM ⁻¹ s ⁻¹	4 to 5.3 μM ⁻¹ s ⁻¹	Microscopy (wild-type and E148A)
ADP-monomer off-rate	Barbed end: 7.2 s ⁻¹ Pointed end: 0.2 s ⁻¹	64 s ⁻¹	Microscopy (catastrophe rate of ATP-ParM)
ATP <i>K_d</i>	1.2 nM	42 nM <i>k</i> ₊ : 0.008 s ⁻¹ <i>k</i> ₋ : 2.32 × 10 ⁵ M ⁻¹ s ⁻¹	ε-ATP fluorimetry
ADP <i>K_d</i>	0.3 nM	2.4 μM <i>k</i> ₊ : 0.56 s ⁻¹ <i>k</i> ₋ : 1.85 × 10 ⁵ M ⁻¹ s ⁻¹	ε-ADP fluorimetry
Hydrolysis rate (estimated)	0.3 s ⁻¹	0.1 to 0.2 s ⁻¹	Modeling
Nucleation rate	1×	300×	Concentration dependence of maximal velocity

high cellular concentrations of ParM (12 to 14 μM) (7), nucleation is unlikely to be the point at which ParM assembly is regulated. It appears that the property of ParM kinetics most amenable to regulation is filament stability. We propose that, at cellular concentrations of ParM, spontaneous nucleation and filament elongation occur throughout the cell, and that these filaments will spontaneously disassemble unless they are stabilized by interaction with ParR-*parC* (8). In this model, only filaments with plasmid bound to both ends are stabilized against catastrophic disassembly (7, 8), and bidirectional elongation of ParM filaments at the interface with the ParR-*parC* complex drives plasmid segregation (Fig. 4B). Such insertional polymerization mechanisms have been proposed for elongating microtubule ends attached to kinetochores and actin filaments bound to formin-family proteins.

References and Notes

1. T. Kruse, J. Møller-Jensen, A. Løbner-Olesen, K. Gerdes, *EMBO J.* **22**, 5283 (2003).
2. H. J. Soufo, P. L. Graumann, *Curr. Biol.* **13**, 1916 (2003).
3. Z. Gitai, N. Dye, L. Shapiro, *Proc. Natl. Acad. Sci. U.S.A.* **101**, 8643 (2004).
4. K. Nordström, L. C. Ingram, A. Lundbäck, *J. Bacteriol.* **110**, 562 (1972).
5. K. Gerdes, S. Molin, *J. Mol. Biol.* **190**, 269 (1986).
6. K. Gerdes, J. E. Larsen, S. Molin, *J. Bacteriol.* **161**, 292 (1985).
7. J. Møller-Jensen, R. B. Jensen, J. Lowë, K. Gerdes, *EMBO J.* **21**, 3119 (2002).
8. J. Møller-Jensen *et al.*, *Mol. Cell* **12**, 1477 (2003).
9. M. Dam, K. Gerdes, *J. Mol. Biol.* **236**, 1289 (1994).
10. F. van den Ent, J. Møller-Jensen, L. A. Amos, K. Gerdes, J. Lowë, *EMBO J.* **21**, 6935 (2002).
11. See supporting data on Science Online.
12. T. Mitchison, M. Kirschner, *Nature* **312**, 237 (1984).

13. H. Wendel, P. Dancker, *Biochim. Biophys. Acta* **915**, 199 (1987).
14. E. Nishida, H. Sakai, *J. Biochem. (Tokyo)* **93**, 1011 (1983).
15. F. Oosawa, M. Kasai, *J. Mol. Biol.* **4**, 10 (1962).
16. E. M. Mandelkow, G. Lange, A. Jagla, U. Spann, E. Mandelkow, *EMBO J.* **7**, 357 (1988).
17. M. F. Carlier, R. Melki, D. Pantaloni, T. L. Hill, Y. Chen, *Proc. Natl. Acad. Sci. U.S.A.* **84**, 5257 (1987).
18. E. C. Garner, C. S. Campbell, R. D. Mullins, data not shown.

19. C. Combeau, M. F. Carlier, *J. Biol. Chem.* **263**, 17429 (1988).
20. L. Blanchoin, T. D. Pollard, *Biochemistry* **41**, 597 (2002).
21. L. Romberg, T. J. Mitchison, *Biochemistry* **43**, 282 (2004).
22. S. Vorobiev *et al.*, *Proc. Natl. Acad. Sci. U.S.A.* **100**, 5760 (2003).
23. D. Panda, H. P. Miller, L. Wilson, *Biochemistry* **41**, 1609 (2002).
24. D. N. Drechsel, M. W. Kirschner, *Curr. Biol.* **4**, 1053 (1994).
25. V. K. Vinson, E. M. De La Cruz, H. N. Higgs, T. D. Pollard, *Biochemistry* **37**, 10871 (1998).
26. M. D. Welch, R. D. Mullins, *Annu. Rev. Cell Dev. Biol.* **18**, 247 (2002).
27. S. H. Zigmond, *Curr. Opin. Cell Biol.* **16**, 99 (2004).
28. M. Pring, M. Evangelista, C. Boone, C. Yang, S. H. Zigmond, *Biochemistry* **42**, 486 (2003).
29. T. J. Mitchison, E. D. Salmon, *Nature Cell Biol.* **3**, E17 (2001).
30. R. B. Jensen, K. Gerdes, *J. Mol. Biol.* **269**, 505 (1997).
31. R. B. Jensen, K. Gerdes, *EMBO J.* **18**, 4076 (1999).
32. We thank members of the Mullins lab for moral support and helpful discussions; L. Frost for R1 plasmid; N. Stuurman and A. Douglas for invaluable assistance with TIRF microscopy; M. Tanegawa for advice on FRET; and T. Mitchison, K. Ryan, R. Vale, M. Dayel, and Q. Justman for critical reading of the manuscript. Supported by NIH grant GM61010-01, Pew Charitable Trust grant P0325SC, and a grant from the Sandler Family Supporting Foundation (R.D.M.). Both E.C.G. and C.S.C. are supported by NSF Predoctoral Fellowships. C.S.C. acknowledges B. Millie for continuing support and advice, and E.C.G. acknowledges B. Zakopyko for being triumphant.

Supporting Online Material

www.sciencemag.org/cgi/content/full/306/5698/1021/DC1
Materials and Methods
SOM Text
Figs. S1 to S4
Movies S1 to S9
References

9 June 2004; accepted 8 September 2004

Accumulation of Mn(II) in *Deinococcus radiodurans* Facilitates Gamma-Radiation Resistance

M. J. Daly,^{1*} E. K. Gaidamakova,¹ V. Y. Matrosova,¹ A. Vasilenko,¹ M. Zhai,¹ A. Venkateswaran,¹ M. Hess,¹ M. V. Omelchenko,^{1,2} H. M. Kostandarithes,³ K. S. Makarova,² L. P. Wackett,⁴ J. K. Fredrickson,³ D. Ghosal¹

Deinococcus radiodurans is extremely resistant to ionizing radiation. How this bacterium can grow under chronic γ radiation [50 grays (Gy) per hour] or recover from acute doses greater than 10 kGy is unknown. We show that *D. radiodurans* accumulates very high intracellular manganese and low iron levels compared with radiation-sensitive bacteria and that resistance exhibits a concentration-dependent response to manganous chloride [Mn(II)]. Among the most radiation-resistant bacterial groups reported, *Deinococcus*, *Enterococcus*, *Lactobacillus*, and cyanobacteria accumulate Mn(II). In contrast, *Shewanella oneidensis* and *Pseudomonas putida* have high iron but low intracellular manganese concentrations and are very sensitive. We propose that Mn(II) accumulation facilitates recovery from radiation injury.

Deinococcus radiodurans is a nonpathogenic, nonsporulating, obligate aerobic bacterium that typically grows in undefined rich

medium (TGY) as clusters of two cells (diplococci) in the early stages of growth and as four cells (tetrads) in the late